Evaluation of a microcompression device for microstructural imaging of bone failure behavior in trabecular bone specimen using HR-pQCT

Elias Jäger, Johannes Pallua, Werner Schmölz

***Abstract*—Many bones within the axial and appendicular skeleton are subjected to repetitive loading during the course of ordinary daily activities. If this loading is of sufficient magnitude or duration, failure of the bone tissue may result. Until recently the structural analysis of these fractures has been limited to two-dimensional sections. Due to the inherent destructiveness of this method, dynamic assessment of fracture progression has not been possible. An image-guided technique to analyze structural failure has been developed utilizing step-wise micro-compression in combination with time-lapsed micro-computed tomographic imaging. For this purpose sample cylinders made of different materials, open cell foam (Sawbone), bone from bovine and red deer were embedded and loaded step-wise. In order to keep the end surfaces of the specimens plane-parallel, a special embedding device was developed. The samples were loaded in different force steps based on results of pretests. Trabecular structure of the deer samples withstood the maximum load of 2000N, the bos tau. bones failed at 1000N and 1500N, the specimens consisting of the 1522-526-01 foam failed at 300 N and the specimens consisting of the 1522-525 foam failed at 550N and 600 N. Post-processing was carried out using the system workstation. The micro-tomography images were used to create three dimensional (3D) models from which various parameters were calculated that provide information about the structure and density of the samples. By superimposing two 3D images and calculating the different surfaces, it was possible to precisely analyse which trabeculae failed in which area and under which load. According to the current state of the art, bone mineral density (BMD) is normally used as a value for bone quality, but the question can be raised whether other values such as trabecular structure, damage accumulation, and bone mineralization can predict structural competence better than BMD alone.**

***Index Terms*—Micro-compression; Micro-tomographic imaging; HR-pQCT; Microstructural bone failure; Bone architecture**

I. Introduction

BONES in the axial and appendicular skeleton undergo repetitive loading during the course of normal daily activities. If this load increases to a sufficient magnitude over a prolonged period of time, it can lead to failure of the bone material [1]. In order to make a detailed analysis of the values at which tissue deformation begins, a dynamic loading process with simultaneous image-guided recording can be used. For this purpose, an image-guided technique for the analysis of structural defects using stepwise microcompression in combination with time-delayed micro-tomographic imaging is being developed. This will allow direct three-dimensional visualization and quantification of fracture initiation and progression at the microscopic level. In addition, this technique can be used to determine and analyze the global failure behavior of the bone tissue.

The ability to determine human bone stiffness is of clinical relevance in many areas, including bone quality assessment and orthopedic prosthesis design. It can be measured using compression testing, an experimental technique commonly used to test bone specimens in vitro [2]. Stiffness can be defined as the resistance of a structure or material to deformation [3]. This property is of great importance in understanding the relationship between structure and function of bone and is clinically relevant in areas such as orthopedic prosthesis design and characterization of bone properties via anatomical sites [4], [5], [6], [7]. Therefore, the ability to accurately and efficiently determine bone stiffness is critical for physicians to understand the effects of factors such as disease, age, and medical interventions on bone quality. The goals of this project are first to develop and fabricate a novel micro-mechanical test system that combines the compression of bone cylinders of cancellous bone material using a specialized load and data acquisition system and simultaneous imaging with a high resolution peripheral quantitative computed tomography (HR-pQCT). Consequently, the test system is validated to perform stepwise load testing of trabecular bone specimens of based on image-guided displacement analysis.

II. Materials and methods

A. Samples

To evaluate the reproducibility and accuracy of the micro-compression test, two types of cellular solids, artificial and biological, are used. For the artificial samples, two groups of three samples each of open cell foam consisting of urethanes, epoxies and structural fillers are used (Manufacturer: Sawbones Europe AB, Sweden). The open-cell structure is often used for biomechanical bone loading tests because its anisotropic and inhomogeneous nature is near to that of human cancellous bone [8]. One group includes samples consisting of the 1522-626-01 foam and one group of the 1522-525 foam. The density and loading characteristics of the two different types of foams are shown in Table I [8]. The biological samples are six lumbar vertebral bodies, three from bovine (*Bos taurus, female, 18 Month*) and three from red deer

*Correspondence to Werner.Schmoelz@i-med.ac.at Assoz. Prof. Dipl.-Ing.(FH) Dr. Werner Schmölz and johannes.pallua@i-med.ac.at, Priv.-Doz. MMag. Dr. Johannes Pallua PhD both University Hospital for Orthopedics and Traumatology, Medical University of Innsbruck, Anichstraße 35, 6020 Innsbruck, Austria

(*Cervus elaphus, male, 3 years*). The vertebral bodies are stored at a temperature of -20°C before testing. Removal of the trabecular bone material is performed differently for the artificial and biological specimens.

TABLE I: Density and load characteristics of the used foam

SKU/Nr.	Density			Compression	
	ASTM D1622		Volume Fraction		
	(pcf)	(g/cc)		Strength (MPa)	Modulus (MPa)
1522-526-1	20	0.32	0.21	1.3	105
1522-525	30	0.48	0.31	3.2	270

B. Sample preparation

Due to the presence of Sawbone material in a rectangular block shape (13 cm x 18 cm x 4 cm), cylindrical specimen can be drilled out directly. For sampling, a diamond tile drill "Silver Power HL" (Manufacturer: Gerätebau Wiedtal Schützeichel GmbH Co. KG, Germany) with vacuum diamond coating is used with an outer diameter of 20 mm and an inner diameter of 15 mm. During the drilling process, the specimen material is completely immersed in water. Subsequently, the drilled out cylinder is shortened to a length of 25 mm using a miter saw. This allows the two Cylinder surfaces to be aligned with each other in a plane-parallel manner.

The biological specimens are slightly thawed and existing muscle and fat tissue is removed using a scalpel. All vertebral processes, such as the proc. spinousus and procc. transversi must be removed for secure mounting of the specimen in the vice. The proximal vertebral body surface is aligned to a horizontal plane that allows a minimum 35 mm hole to be drilled centrally through the vertebral body. To cool the drill tip and ensure a clean cut surface, the clamped vertebral body together with the vice is placed in a water bath. If complete cannulation of the vertebral body is not possible, excess bone tissue must be removed afterwards until only the drilled-out cylinder remains. Since only trabecular bone material is to be used, the cortical layers of the specimen cylinder must be removed. As with the artificial specimens, the biological cylinder specimen is also cut to a length of 25 mm. To ensure plane parallelism, a conventional hand saw in combination with a saw gauge (preferably made of plastic for later cleaning) is used for cutting. The removed cylinder of trabecular bone tissue is packed in special storage bags, labeled and stored at temperatures of -20°C to ensure the integrity of the trabecular structures. Removed bone, fat, tendon, and muscle tissue is also frozen and later disposed of in an appropriate manner. Before the biological cylinder specimen can be used for the further course of the experiment, they must be thawed 24 h before embedding. In setting up the experiment, we followed the experiment procedure of Nazarian and Müller, 2004 [9].

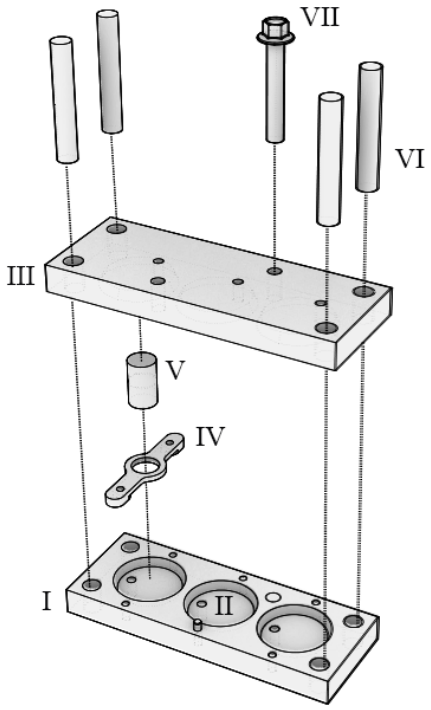

Fig. 1: Embedding device; I ... Base Plate; II ... Depression; III ... Cover Plate; IV ... Centering Aid; V ... Specimen Cylinder; VI ... Rods; VII ... Adjustment screw (M6)

C. Sample embedding

To ensure that the direction of the applied force on the surfaces of the cylinder ends is uniform when the specimens are loaded, these surfaces must be plane-parallel. However, since the specimens cannot simply be placed in the load model, they must first be embedded at both ends. It must be ensured that the surfaces of the embedding material correspond to the cylinder end surfaces. In order to meet these requirements, a special embedding device was designed which also allows three specimens to be embedded simultaneously. The embedding device consists of several components which are used depending on the stage of embedding. A base plate (figure 1, I), in which three circular downwards tapered depressions (figure 1, II) with a depth of 5 mm were made, a cover plate (figure 1, III) which is the counterpart to the base plate and has exactly the same structure, and three centering aids (figure 1, IV) with an inner diameter of 15 mm, one for each depression. The wells were designed that the inner diameter matches the diameter of the specimen cylinders (figure 1, V).

In the first step of the mounting process, the conical wells are sprayed with wax release spray (Wachstrennspray, Gößl Pfaff GmbH, Karlskorn) and filled with the mounting material (Huntsman Advanced Materials GmbH, Switzerland; Mixture of RenCast® FC 53 Polyol, RenCast® FC 53 Isocyanat and binders), the centering aids are positioned on the designated pegs and the specimens are pressed through the centering aids into the mounting material. The recesses of the cover plate are positioned with cylindrical rods (figure 1, VI) directly above

the specimens and serve as a weighting of the specimens so that they are not displaced during the curing process of the embedding material. In addition, a flattened M6 screw (figure 1, VII) with a length of 50 mm can be used to increase the distance between the base and the cover plate. This serves to reduce the weight force on sensitive samples. After 30 minutes of curing at room temperature, the centering aids and the cover plate can be removed again. In the next mounting step, the depressions of the cover plate are filled with mounting material and the base plate with the specimens already mounted on one side is positioned again with the aid of the cylindrical rods so that the specimen tips protrude into the mounting material on the other side. After a further 30 minutes of curing, the two plates can be removed again and three cylindrical specimens, each embedded at the ends, can now be set to the load model in a special fixture and used for the further course of the experiment.

D. Loading device

In order to stepwise load the cylindrical specimens in the XtremeCT II, a special loading model is required, which can be fixed in the HR-pQCT system. As part of her bachelor's thesis, Debout [10] constructed just such a compression device. The basic structure consists of three steel plates; front, rear and center plate (figure 2; I, II, III). The front and rear plates are connected by three cylindrical carbon rods (figure 2, IV) and form the basic structure. Special reference ball pivots (figure 2; V) are attached to both plates, from which the compression device can be suspended in the XtremeCT II. The ball pivots represent the only contact surface to the XtremeCT II. Suspended on the carbon rods is the center plate, which can be moved freely along the rods and represents the force transmission. For the adjustment of the force intensity, a threaded spindle (figure 2; VI) fixed via a spindle nut (figure 2; VII) leads from the back plate to the center plate. The center plate is thus moved in translation depending on the torsional moment of the spindle. For force measurement, a load cell (figure 2; VIII) is centrally mounted on the center plate. Together with a special loading head and the force transmission from the torsional moment into a translational movement, they form the loading unit that can specifically compress the specimen and simultaneously record the applied force. Additionally a Measuring device for displacement, called LVDT (figure 2; IX) is placed between the back plate and the center plate which has to be zeroed before a load test and records the displacement of the load unit. The load cell and the displacement measuring device were connected to a Amplifier System (PICAS Multi Channel Amplifier) from Peekel (PEEKEL Instruments GmbH, Bochum, Germany). Which amplifies the measurement data and displays it in real time. In this way, it is possible to follow how much force is acting on the clamped sample and how much the loading head has already shifted axially [10]. In contrast to the basic load testing of whole vertebral body units with the compression device, the specimens of the present experiment have to be fixed with a modified form of the mounting structure due to their smaller size. For this purpose, a recess of 10 mm with a diameter of 40 mm was milled into a circular block of embedding material, in the course of which the embedded specimen cylinders (outer diameter of the embedded cylinder tips = 40 mm) can be inserted directly into the recess. The cylindrical block of embedding material is accordingly screwed to a flange (figure 2, X), which in turn is attached in the compression device to a mounting mechanism (figure 2, XI) specified for this purpose.

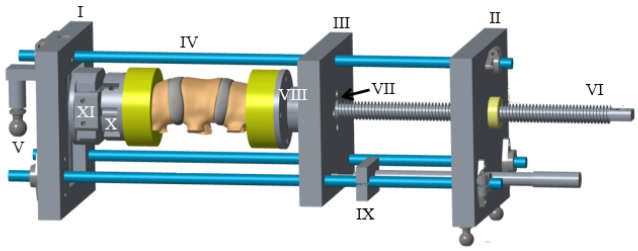

Fig. 2: Structure of the compression device; I ... Front Plate, II ... Rear Plate, III ... Center Plate, IV ... Carbon Rods, V ... Ball Pivots, VI ... Spindle, VII ... Spindle Nut, VIII ... Load Cell, IX ... LVDT, X ... flange, XI .. Mounting Mechanism; Adapted from [10]

E. Micro-tomographic imaging

XtremeCT II from the Scanco company (Scanco Mecial AG, Brüttisellen, Switzerland) was used to for micro-tomographic imaging. This system is specifically designed to perform high resolution peripheral quantitative computed tomography on the distal tibia and radius in humans for *in vivo* clinical assessment of osteoporosis. A low X-ray dose allows regular follow-up measurements, and powerful True-3D assessment software automatically matches cortical and trabecular bone regions to previous measurements for direct comparison of density and structural features. It can also be used in preclinical studies to scan large bones or bone segments at 61 µm (nominal isotropic voxel size) resolution. Which represents a significant improvement in resolution compared to the first generation with a isotropic voxel size of 82 µm. Clinical HR-pQCT was used in this study to visualize the change in trabecular structure during compression. The parameters in HR-pQCT were developed based on the assumption that the mechanical properties of the trabecular structure depend not only on the density of the material but also on the specific distribution of the struts, the trabecular network [11], [10].

F. Experimental set-up and implementation

In order to be able to recognise the course of the trabecular change in the later HR-pQCT scans, different loading steps were determined for the different sample types based on their density properties. For this purpose, one specimen each (Bos tau., cervus el., SB-525, SB-526) was preloaded with a loading machine (MTS, 858 MiniBionix II, MN, USA), which records the force and the axial displacement. The actual stress test consists of an image-guided procedure that visualises the structural defects by stepwise micro-compression

using the compression device in combination with HR-pQCT imaging. Therefore the compression device is suspended from the XtremeCT II via the ball pivots and the load cells are connected to the amplifier system and calibrated (figure **??**, I). The specimen is placed in the cylindrical block of embedding material and loaded with a preload of 50 N. The cylindrical specimen form an axis with the threaded spindle as shown in figure **??**, II. Subsequently the load model and the clamped sample are pushed into the XtremeCT and the first scan is performed. Once the scan is complete, the load is set to the defined steps using the PICAS display. Therefore the threaded spindle is turned to increase the axial force to the defined steps. This process is repeated until the trabecular structure of the sample yields.

G. Image post-processing

Regarding the post-processing, the focus was on creating 3D images of the HR-pQCT scans using the internal system-workstation. Which includes multiprocessing virtual memory-based operating system (VMS) (Hewlett-Packard, Palo Alto USA) in combination with a internal processing language (IPL) (Scanco Medical AG, Brüttisellen, Switzerland). For this purpose, the desired volume of interest (VOI) was selected layer by layer from the HR-pQCT scans and 3D images were reconstructed. The process additionally calculates various parameters from the VOI that can be used for the comparison of BMD and trabecular structure. The calculated parameters of the VOI are composed of the following: total volume (TV), bone volume (BV), relative bone volume (BV/TV), connectivity density (CD), structure model index (SMI), trabecular number (Tb.N), trabecular spacing (Tb.Sp) and the Mean/Density of the BV. TV represent the VOI volume and is measured in mm³. The Bone Volume (BV, [mm³]) is calculated analytically with a formula (Eq. **??**) [12].

BV is calculated using a tetrahedron meshing technique, which in turn is generated by the so called marching cubes method. [12]

$$SMI = 6 \cdot \frac{(\frac{dS}{dr})BV}{BS^2} \tag{1}$$

The structure modelling index provides information about the structure of the trabeculae inside the sample cylinders. When calculating the SMI, the bone surface (BS) is expanded by an infinitesimal magnification and then compared to the volume. Therefore a network of triangles is attached to the bone area (BA) and summed up to determine the BS. Now the surface is expanded a short distance (dr) and measured again. This change in surface (dS) is now divided by dr, which corresponds to an approximal derivative of the surface area, and multiplied by the BV to determine the final SMI. The SMI distinguishes between three characterisations of the trabecular bone structure, spheres (SMI=4), rods (SMI=3) and planes (SMI=0) [13]. The Tb.N can be defined as the occurrence of intersections between bone and non-bone material per a defined length (1/mm). Further information about the properties of the trabecular structure is provided by the Trabecular Thickness (trabecular thickness (Tb.Th), [mm]) and the Trabecular Separation/Spacing (Tb.Sp, [mm]), the properties are calculated via the relationships in equation 3, 3 and 4.

$$Tb.N = \frac{BS}{2 \cdot TV} \tag{2}$$

$$Tb.Th = 2 \cdot \frac{BV}{BS} \tag{3}$$

$$Tb.Sp = 2 \cdot \frac{TV - BV}{BS} \tag{4}$$

H. Determination of trabecular change under load

By superimposing two 3D images of the same test cylinder with different loads, structural changes in the trabeculae are made visible. It can be visually understood at which load and at which point the trabecular bone material changes or fails. For this purpose the transformation matrix of the base image (3D image of the specimen with 50N load) was created. To determine the exact trabecular structure change or failure, horizontal two dimensional (2D) slices were calculated from the superimposed 3D images. These layers can provide a detailed statement of the location and load at which the highest change occurred. The areas were determined using MATLAB. The DICOM files of the 3D images were loaded into the program. The areas could then be analyzed using a self-created function ”matCalc”, which determine three different surface values and sum up all values of one kind in one Matrix. The calculated data were exported as Excel tables.

III. Results

The workflow of the microcompression test system resulting from the materials and methods is given in the appendix in figure 7.

A. Load levels definition

With regard to the preloading of the specimens, all types show different maximum forces load of failure (LOF) until the break of the trabecular structure. Table 3 illustrates the result of the load test with the MTS as well as the resulting load steps for the stress test inside the MicroCT. Figure 3 shows the loading curve of the bos tau. cylinder specimen. Therefor the course of the axial force and the axial displacement over time is shown.

TABLE II: Load of failure of one specimen each and the resulting load steps

SampName, Nr.	LOF [N]	Load steps [N]
Cervus elaphus, L4	1758	50 - 1000 - 1500 - 1750 - 1800
Bos Taurus, L4	4767	50 - 1000 - 1500 - 1750 - 2000
SB 1522 525, 03	640	50 - 400 - 500 - 600 - 700
SB 1522 526, 03	360	50 - 200 - 250 - 300 - 400

TABLE III: Parameters of bos tau., cervus el. and bone surrogate samples in Comparison

SampName	BV/TV [%]	Conn-Dens	TRI-SMI	Tb.N [mm]	Tb.Th [mm]	Tb.Sp [mm]	MatDens [mgHA/ccm]
Cervus elaphus. [50 N]	41.17 ± 6.83	1.347 ± 0.428	-1.759 ± 0.688	1.508 ± 0.123	0.356 ± 0.054	0.598 ± 0.054	727.07 ± 23.85
Cervus elaphus. [1000 N]	40.81 ± 6.76	1.346 ± 0.414	-1.718 ± 0.690	1.508 ± 0.122	0.360 ± 0.052	0.599 ± 0.052	726.48 ± 22-49
Cervus elaphus. [1500 N]	40.83 ± 6.69	1.327 ± 0.407	-1.704 ± 0.700	1.500 ± 0.114	0.361 ± 0.052	0.601 ± 0.051	725.02 ± 21.22
Cervus elaphus. [1750 N]	40.91 ± 6.61	1.314 ± 0.384	-1.681 ± 0.666	1.483 ± 0.100	0.363 ± 0.050	0.609 ± 0.043	726.97 ± 17.91
Cervus elaphus. [2000 N]	41.56 ± 6.24	1.314 ± 0.388	-1.638 ± 0.691	1.429 ± 0.036	0.366 ± 0.048	0.639 ± 0.004	725.61 ± 18.30
Bos Taurus [50 N]	35.33 ± 3.76	4.921 ± 0.288	0.284 ± 0.249	1.596 ± 0.02	0.279 ± 0.033	0.606 ± 0.003	610.16 ± 5.45
Bos Taurus [1000N]	36.02 ± 4.12	4.949 ± 0.104	0.232 ± 0.295	1.595 ± 0.004	0.280 ± 0.028	0.603 ± 0.006	609.67 ± 5.94
SB 1522 525 [50N]	18.69 ± 1.29	0.435 ± 0.016	1.376 ± 0.256	0.583 ± 0.002	0.508 ± 0.020	1.762 ± 0.025	596.04 ± 2.43
SB 1522 525 [400N]	18.57 ± 1.30	0.440 ± 0.013	1.436 ± 0.250	0.583 ± 0.003	0.509 ± 0.023	1.762 ± 0.024	594.58 ± 4.28
SB 1522 525 [500N]	18.61 ± 1.50	0.439 ± 0.021	1.432 ± 0.270	0.586 ± 0.003	0.512 ± 0.025	1.760 ± 0.017	594.68 ± 5-35
SB 1522 525 [600N]	19.02 ± 1.68	0.528 ± 0.107	1.865 ± 0.161	0.607 ± 0.016	0.500 ± 0.002	1.698 ± 0.028	593.51 ± 1.85
SB 1522 526 [50]	15.66 ± 0.42	1.215 ± 0.142	0.798 ± 0.060	0.535 ± 0.008	0.316 ± 0.005	1.986 ± 0.029	634.98 ± 4.19
SB 1522 526 [200N]	15.66 ± 0.36	1.206 ± 0.115	0.805 ± 0.051	0.537 ± 0.006	0.316 ± 0.004	1.974 ± 0.023	634.69 ± 4.28
SB 1522 526 [250N]	15.78 ± 0.40	1.243 ± 0.120	0.820 ± 0.032	0.541 ± 0.009	0.315 ± 0.004	1.963 ± 0.033	634.01 ± 4.77
SB 1522 526 [300N]	16.17 ± 0.41	1.254 ± 0.130	0.858 ± 0.048	0.565 ± 0.011	0.315 ± 0.004	1.881 ± 0.46	633.13 ± 5.06

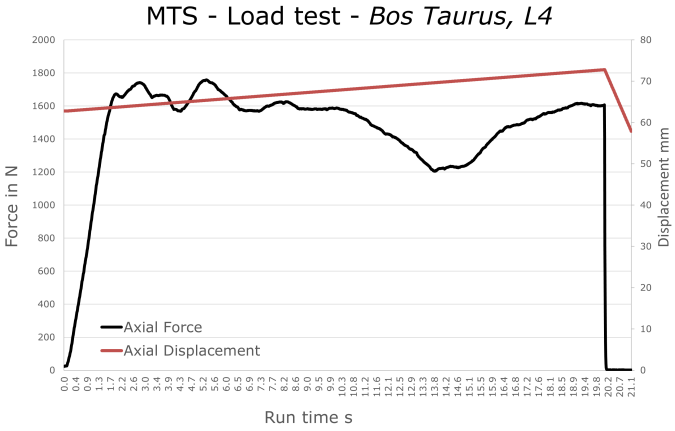

Fig. 3: Example of an MTS load curve

B. Micro-compression tests

During the load tests in the XtremeCT II, the cervus el. bones withstood up to the last load step (2000 N) and the LVDT returned displacement values of 29 mm and 30 mm. The loading head was thus displaced transversely and the bone specimen was shifted or compressed by this value. Thus, no direct fracture progression could be detected on the HR-pCT scans. However, the trabecular structure showed small changes near the embedded sites. The compression device already shows vertical bending at a load of 2000 N. The bone structure of the bos tau. specimens broke at a load of 1000 N and 15000 N with a displacement of the loading head by 20 and 26 mm. The bone surrogate cylinder samples showed significantly lower stability than the biological samples. Both specimens consisting of the 1522-526-01 foam failed already at 300 N with displacement values of 10 mm and 16 mm. The other two Sawbone specimens from the 1522-525 foam withstood a load of 550 N and 600 N with a transverse displacement of the loading head of 9.4 mm and 12.9 mm. Basically, all cylinder specimens were loaded to failure. If all specimens had endured to maximum loading, there would be five scans of each specimen. However, since all but the cervus el. specimens failed at one of the specified loading steps, the number of scans available is not the same for all. The trabecular structural change can already be analyzed very well when comparing the preloaded (50 N) with the failure load. Each further intermediate step gives even more detailed information about the structural change over the increasing load. The most important parameters calculated by the HR-pQCT software from the scans and the resulting 3D images are listed in table III. The mean value and the standard deviation (SD) of the samples are shown in each case. Figure 4 visualises an example of a embedded specimen before and after loading as well as reconstructed 3D images with the correlated cross-section before and after loading with LOF.

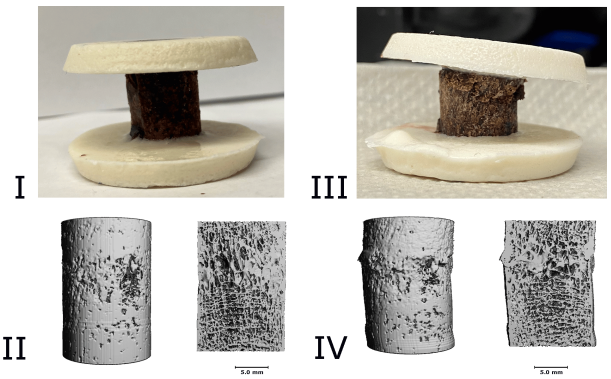

Fig. 4: Embedded sample before (I) and after (II) the stepwise micro-compression test. 3D model with cross-section of an unloaded specimen (III) and a 3D model at failure load with cross-section (IV).

C. Superimposition of two 3D images

The aim of overlaying two 3D images was to show the changes of the trabecular bone structure in three dimensional space on the one hand and to use horizontal layers of these images on the other hand in order to determine the areas of the overlay and the superimposed area. Due to the fact that a 3D image was calculated from the HR-pQCT scans for each load step, all levels can therefore be compared with the initial sample cylinder. This in turn provides a precise insight into the structural change of the sample trabeculae at each loading step like in figure 5, where a overlay of two 3D-Images of an specimen cylinder is shown.

In order to make a precise statement about the structural change of the trabeculae via the increasing force, the super-

imposed 3D images must be split into horizontal 2D slices. In figure 6 eleven layers of a 3D image superimposition is shown. The number of layers is based on the size of the 3D image, in the example image (figure 6) the number of layers is 370. At the ends of the sample cylinders, the superimposition of two 3D images of different loads does not normally provide any information about the change or failure of the trabecular structure, since the more heavily loaded sample is always compressed and thus smaller than the initial sample. Therefore, the layers without significance (for example (*exempli gratia*) (e.g.) only the initial sample can be seen) had to be filtered out during the evaluation (in figure 6, slices 1 - 40 and 340 - 370). Depending on the change or failure of the trabecular structure, each layer shows a different behaviour, which can be seen by calculating the different proportions of the two 3D images and the overlay area.

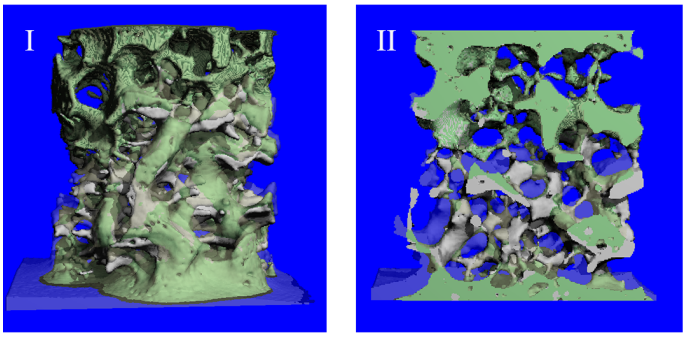

Fig. 5: Overlay of two 3D images, acquired from step-wise testing of a SB 526 specimen at 50 N an 300 N; I ... front view, II ... inside view

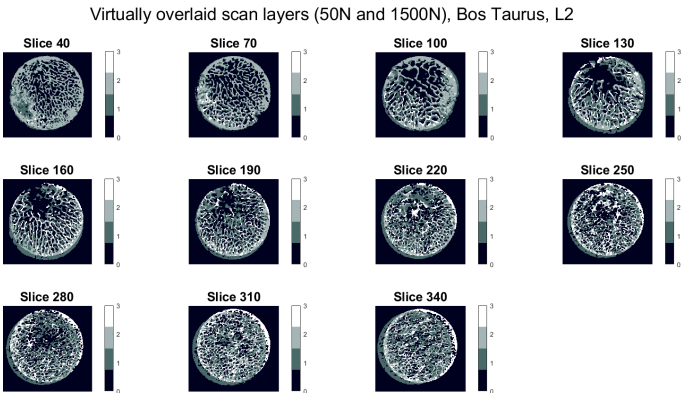

Fig. 6: Layers of the superimposed 3D images indices and correlated colours of the different regions; 0 ... background, 1 ... sample 3D image (1500N), 2 ... overlay area, 3 ... initial

IV. Discussion

Focusing at the structural parameters in table III, it is noticeable that the BMD values hardly differ and a clear statement as to whether changes in the trabecular structure up to fractures occur is impossible. It must be mentioned that the small number of samples, and the associated high standard deviation makes a clear statement about changes in relation to all parameters very difficult. Nevertheless, HR-pQCT specific parameters have shown small changes in some samples, especially at the highest loading level. The connectivity density of the trabeculae and the fraction of bone volume increases, especially for the artificial samples, at higher loadings. This can be explained by the fact that the trabeculae are pressed into each other, the Tb.N become smaller and the BV increases. Another significant value is the SMI, which describes the shape of the trabeculae. It clearly shows the different trabecular shapes of the biological samples (values between 0.84 and -1.759), which rather indicates concave shapes ($<$ 0), compared to the artificial samples which rather show mixture of planar and cylindrical shapes (values between 0.798 and 1.865). However, a distinct trabecular shape cannot be attributed to the specimens when analyzing the results of the structure model index values (Values not correspond to a specific SMI value, [0, 3, 4]). Here probably the mean ellipsoid factor (EF), fitting ellipsoids in three dimensional space, could give better information as described in the work of salmon2015. The trabecular shape difference is also evident when comparing the 3D models and their sectional views with those of the biological samples. The artificial specimens have significantly larger trabecular distances (Tb.Sp 1.762 - 1.986) than the biological ones (Tb.Sp 0.279 - 0.366), resulting in the biological specimens withstanding significantly more strain. In connection with the load, the samples of the cervus el. material again withstood significantly more than the bos tau. samples, which is possibly due to the fact that wild animals are exposed to higher external loads in everyday life than bovine. On the one hand, however, bovine weigh significantly more than deer, which corresponds to a greater permanent load on the spine. On the other hand, they have more massive and wider vertebral bodies, which may be better able to distribute the weight force.

All in all, the evaluation of the load tests has shown that the structural parameters generated by the HR-pQCT software describe the properties of the investigated bone material. In addition, the combination of the micro-compression test with subsequent HR-pQCT scans can also provide information about the behavior of trabecular bone material under stepwise increasing load. Comparing the micro-compression device for dynamic image-guided failure assesment of levchuk2018 with the test system developed in this work, the advantage of using the compression device developed from elisabeth2017 for stepwise loading and the HR-pQCT system for microscopic microscopic imaging is clear. On the one hand, a 3D model can be reconstructed from each scanned sample, in which moreover any cross-section can be taken in order to investigate the exact trabecular structures, and on the other hand, the samples can be loaded with axial forces of up to 2000 N.

With regard to other techniques that have investigated local bone changes under load, the work of Nazarian and Müller, 2003 nazarian2003 is a good comparative literature. They loaded whale bone specimens and aluminium foams to failure loading and used micro computed tomography (µCT) for image processing. Compared to the HR-pQCT, µCT the X-ray source does not rotate around the sample to be measured but is fixed and the sample holder rotates around itself. µCT has a significantly higher radiation exposure and is

therefore not suitable for human and clinical use [14]. In contrast to the specimens used (diameter 15 mm, length 25 mm) in the present work, they used smaller cylindrical bone specimens (diameter 8 mm, length 16 mm) which they loaded to ultimate strength 16.185 MPa (whale specimens) and 2.108 MPa (aluminium foam specimens with the highest density). MPa equals N/mm² which, with a sample diameter of 8 mm, means that the whale samples were loaded with about 813 N and the aluminium samples with about 105 N axial force. Applying these calculations to the diameter of the specimens here, the result is 2860.13 N for the whale specimens and 372.51 N for the alumium specimens. There are therefore very similarities in terms of LOF, with the whale samples between the biological samples in this work and the alumium foam with the highest density having almost the same ultimate loading as the SB-526 samples. Like the result of this work, the work of Nazarian and Müller, 2003 [9] also shows that the quality and the associated trabecular geometry of the bone material may be better assessed if, in addition to BMD, the structural composition of the bone, the accumulation of fractures and bone mineralization are also taken into account. The applied method of superimposing the generated 3D models showed significant advantages in terms of localization of the change in trabecular structure induced by loading. It is possible to compare each individual layer of a 3D image with another one of the same sample under a higher load and makes it possible to infer from which load in which layer the greatest change in trabecular structure occurred. In the case of the artificial samples, this method clearly showed that trabecular changes already occurred in some layers before the failure load. In the evaluation of structural parameters, this conspicuousness is nowhere to be seen.

V. Conclusion

The overall goal of this project was, first, to develop a micro-mechanical testing system consisting of a compression fixture and high-resolution three dimensional imaging, and second, to validate the testing system together with the high-resolution imaging by stepwise loading of bone and bone surrogate specimens. The development of the micro-mechanical test system was successfully implemented using a special compression device and a HR-pQCT system. The subsequent validation was carried out on the one hand with cylindrical samples from bovine and red deer bone material and on the other hand with cylindrical bone samples from two bone surrogate with different densities and stability properties. Due to the special shape of the clamping device of the compression model, a special embedding device made of stainless steel had to be consulted for the validation of the system, which allows the embedding of 3 specimens at the same time. Furthermore, the reconstructed 3D models with the internal HR-pQCT were virtually overlaid and evaluated. Individual layers of all samples were visualised and analysed. The change in the trabecular network up to fractures occurring under stepwise loading can be determined layer by layer as well as the resulting areas.

In order to adapt the micro-compression testing system for clinical questions, it would be advantageous in the first instance to carry out the validation process described here with human bone cylinders (sample quantity of approximately 10 trabecular bone cylinders). The next step would be to perform the HR-pQCT test with samples from degenerative diseased bone material (e.g. osteoporosis) in order to subsequently determine differences between the behaviour of healthy and diseased bone tissue under load in a statistical evaluation. Together with the workflow of the designed micro-compression system, the interpretation of the results and the statistical evaluation, a finite element model could be created that simulates the designed test system. This would make it possible to analyse human trabecular bone structure on a microscopic level without removing bone tissue. Furthermore, in addition to the information about the trabecular geometry of the bone structure, degenerative bone diseases such as osteoporosis, cancellous arthritis, tumours in the bone tissue could be possibly detected earlier. From the resulting load simulation and the reconstructed 3D models, it could also be determined where changes or fractures occur in the bone tissue and the treatment could be adapted based on these results.

APPENDIX A
WORKFLOW OF DESIGNED MICRO-COMPRESSION TESTING SYSTEM

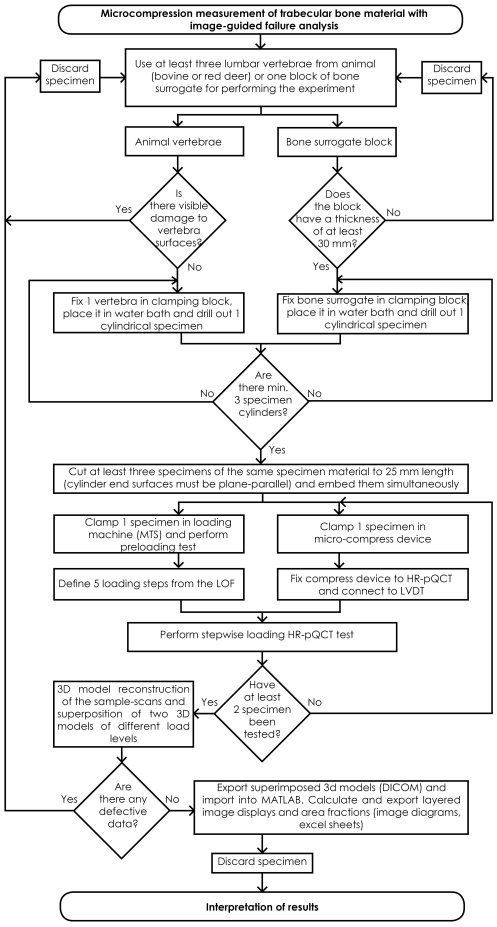

Fig. 7: Recommended workflow for micro-compression measurement of trabecular bone material with designed testing system

ACKNOWLEDGMENT

The authors would like to thank Ephräm Unterberger and Thomas Wechselberger both from the Österreichische Bundesforste for their aid in sample collection. We owe thanks also to Gerald Degenhart BSc. MSc. from Department of Radiology, Medical University of Innsbruck, Austria, for his aid in data analyses.

REFERENCES

[1] R. J. Klinck, G. M. Campbell, and S. K. Boyd, "Radiation effects on bone architecture in mice and rats resulting from in vivo micro-computed tomography scanning," *Medical Engineering Physics*, vol. 30, no. 7, pp. 888–895, 2008. [Online]. Available: https://www.sciencedirect.com/science/article/pii/S1350453307001889

[2] S. Zhao, M. Arnold, S. Ma, R. L. Abel, J. P. Cobb, U. Hansen, and O. Boughton, "Standardizing compression testing for measuring the stiffness of human bone," *Bone & Joint Research*, vol. 7, no. 8, pp. 524–538, 2018, pMID: 30258572. [Online]. Available: https://doi.org/10.1302/2046-3758.78.BJR-2018-0025.R1

[3] A. Miles and S. Gheduzzi, "Basic biomechanics and biomaterials," *Surgery (Oxford)*, vol. 30, no. 2, pp. 86–91, 2012, orthopaedics I: General Principles. [Online]. Available: https://www.sciencedirect.com/science/article/pii/S0263931911002468

[4] H. E. Rubash, R. K. Sinha, A. S. Shanbhag, and S. Kim, "Pathogenesis of bone loss after total hip arthroplasty," *Orthopedic Clinics of North America*, vol. 29, no. 2, pp. 173–186, 1998. [Online]. Available: https://www.sciencedirect.com/science/article/pii/S0030589805703163

[5] P. Augat, T. Link, T. F. Lang, J. C. Lin, S. Majumdar, and H. K. Genant, "Anisotropy of the elastic modulus of trabecular bone specimens from different anatomical locations," *Medical Engineering Physics*, vol. 20, no. 2, pp. 124–131, 1998. [Online]. Available: https://www.sciencedirect.com/science/article/pii/S1350453398000010

[6] A. Nazarian, D. von Stechow, D. Zurakowski, R. Müller, and B. D. Snyder, "Bone volume fraction explains the variation in strength and stiffness of cancellous bone affected by metastatic cancer and osteoporosis," *Calcified tissue international*, vol. 83, no. 6, p. 368—379, December 2008. [Online]. Available: https://doi.org/10.1007/s00223-008-9174-x

[7] A. Ciarallo, J. Barralet, M. Tanzer, and R. Kremer, "An approach to compare the quality of cancellous bone from the femoral necks of healthy and osteoporotic patients through compression testing and microcomputed tomography imaging," *McGill journal of medicine : MJM : an international forum for the advancement of medical sciences by students*, vol. 9, pp. 102–7, 07 2006.

[8] "Sawbones general catalog," accessed: 2021-06-20. [Online]. Available: https://www.sawbones.com/media/assets/product/documents/general-catalog.pdf

[9] A. Nazarian and R. Müller, "Time-lapsed microstructural imaging of bone failure behavior," *Journal of Biomechanics*, vol. 37, no. 1, pp. 55–65, 2003. [Online]. Available: https://www.sciencedirect.com/science/article/pii/S0021929003002549

[10] E. L. Debout, "Test rig for (ec)-centric vertebrae compression in a hr-pqct," Bachelor's Thesis, University of Applied Sciences Ulm.

[11] S. L. Manske, Y. Zhu, C. Sandino, and S. K. Boyd, "Human trabecular bone microarchitecture can be assessed independently of density with second generation hr-pqct," *Bone*, vol. 79, pp. 213–221, 2015. [Online]. Available: https://www.sciencedirect.com/science/article/pii/S8756328215002422

[12] W. E. Lorensen and H. E. Cline, "Marching cubes: A high resolution 3d surface construction algorithm," *SIGGRAPH Comput. Graph.*, vol. 21, no. 4, p. 163–169, Aug. 1987. [Online]. Available: https://doi.org/10.1145/37402.37422

[13] P. L. Salmon, C. Ohlsson, S. J. Shefelbine, and M. Doube, "Structure model index does not measure rods and plates in trabecular bone," *Frontiers in Endocrinology*, vol. 6, p. 162, 2015. [Online]. Available: https://www.frontiersin.org/article/10.3389/fendo.2015.00162

[14] B. Zhou, *Bone Quality Assessment Using High Resolution Peripheral Quantitative Computed Tomography (HR-pQCT)*. Columbia University, 2015.